

## Microstructure and formation mechanism of in-situ TiC-TiB<sub>2</sub>/Fe composite coating

WANG Zhen-ting(王振廷), ZHOU Xiao-hui(周晓辉), ZHAO Guo-gang(赵国刚)

College of Materials Science and Engineering,  
Heilongjiang Institute of Science and Technology, Harbin 150027, China

Received 19 November 2007; accepted 4 April 2008

**Abstract:** Steel matrix composite coatings locally reinforced with in situ TiC-TiB<sub>2</sub> particulates were prepared by argon arc cladding(AAC) with different mass fractions of Fe and Ti+B<sub>4</sub>C powders as the binding materials. The microstructure, micro-hardness and wear resistance were investigated using SEM, XRD, Micro-hardness Tester, and Friction and Wear Tester, respectively. The results show that the main phases of coating are TiC, TiB<sub>2</sub> and  $\alpha$ -Fe. The excellent metallurgical bonding is formed between the composite coating and substrate. The coating is uniform, continuous and almost defect-free and the particles are dispersively distributed in the clad coating. Moreover, the formation mechanism was investigated. With the increase of the content of TiC+TiB<sub>2</sub>, the micro-hardness and wear resistance are also improved at the room temperature under normal atmosphere conditions.

**Key words:** TiC-TiB<sub>2</sub>; argon arc cladding; microstructure; formation mechanism

### 1 Introduction

Titanium alloy matrix composites have received considerable interest due to their high strength/mass ratio, elevated temperature resistance and excellent corrosion resistance[1–3]. Recently, however, iron and steel matrix composites reinforced with in situ synthesized ceramic particulates have been the subject of significant investigation, which have low costs and exhibit good mechanical properties[4–5]. Among these ceramic particulates, TiC and TiB<sub>2</sub> are obtaining more attention due to their high melting points, low densities, good thermal and chemical stability, and high hardness[5–6]. These facts make them attractive as aircraft propulsion systems and cutting tools. Moreover, they can be used as cathodes for Hall-Heroult cell due to their good electrical conductivity[7–9].

Several methods have been used for the preparation of TiC-TiB<sub>2</sub> compositions, such as mechanical alloying [7], spark plasma synthesis(SPS)[8], high-energy ball milling[9], and self-propagating high temperature synthesis(SHS) [10–11]. Mechanical alloying was used to synthesize TiC-TiB<sub>2</sub> composites after milling for

90 min[7], and with further milling, the diameters of the composite powder rarely change but the crystalline sizes decrease gradually. The SPS was used to synthesize dense TiC-TiB<sub>2</sub> composites starting from Ti, C and B<sub>4</sub>C powders by LOCCI et al[8] who obtained a pure dense product(relative density 98%). It can be seen that the researches of TiC-TiB<sub>2</sub> mainly focus on composites, and there are few coatings.

Argon arc cladding (AAC) is a new method for fabricating composition, which uses tungsten inert gas welding(TIG). Compared with those methods mentioned, the equipment of AAC is cheaper, easy to operate and popularize, and has engineering practical value[12–15]. Recently, new attempts have been made using AAC to achieve surface composites or surface alloying[16–17]. WANG et al[17] investigated the multi-pass overlapping gas tungsten arc welding (GTAW) with graphite and ferrotitanium (Fe, Ti) on AISI 1020 steel, and the composite coating exhibited high hardness and excellent wear resistance. Up to now, there has no report about in-situ synthesized TiC-TiB<sub>2</sub>/Fe composite coating using argon arc cladding(AAC). In this work, in-situ TiC-TiB<sub>2</sub>/Fe composite coating was synthesized using AAC, which can provide basic experimental and academic

reference, at the same time, the microstructure and formation mechanism were investigated as well.

## 2 Experimental

Q235 steel was used as the substrate material, and the dimension was 40 mm × 20 mm × 10 mm. The starting materials were Ti 99.5%, B<sub>4</sub>C 99.5% and Fe powders, and the component ratios of coatings are listed in Table 1. The total mass of every sample was 4 g. The powders were mixed symmetrically to make up a powder mixture as the raw coating alloy. Then the mixed powders were pre-placed on the surface of Q235 steel using as a small amount of soluble glass as possible to keep the powders on the surface of the substrates tight. Powders and substrates were thoroughly cleaned, dried and finally rinsed by acetone with the thickness of about 1 mm, and left about 1 mm of either end as the place to ignite arc. The samples were first put in the ventilated place at the room temperature for 24 h and then dried at 100 °C for about 1 h by DZ-2BC Vacuum Dryness Oven. Then coatings were carried out by MW3000 Digital Tungsten Inert Gas welding(TIG) machine with the operating welding current 140 A, welding voltage 20–22 V, argon flow rate 10 L/min, and welding speed 125 mm/min. The TIG welding process is shown in Fig.1[18].

**Table1** Component ratios of coating (mass fraction, %)

| Sample No. | Fe | Ti | B <sub>4</sub> C |
|------------|----|----|------------------|
| 1          | 30 | 50 | 20               |
| 2          | 50 | 30 | 20               |
| 3          | 60 | 20 | 20               |
| 4          | 70 | 20 | 10               |

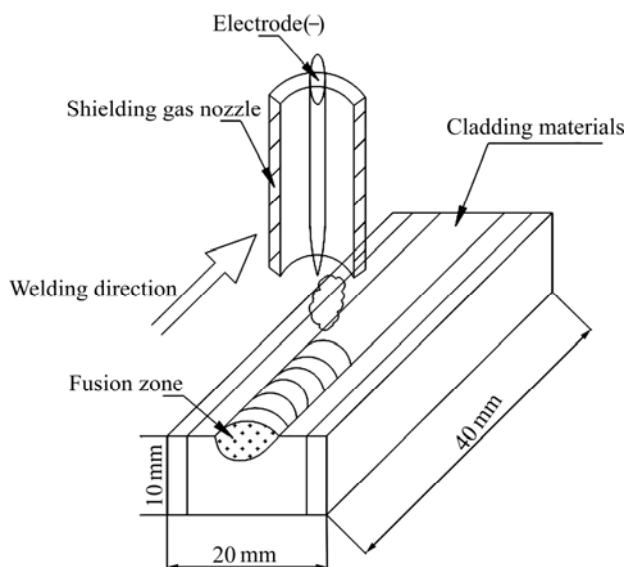


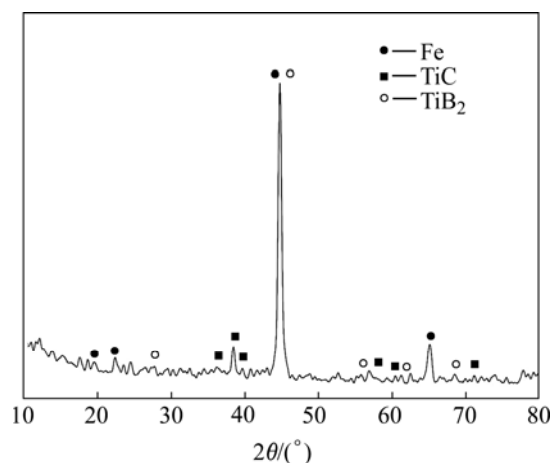
**Fig.1** Schematic representation of TIG welding clad process and coating layer

The microstructures of coatings were examined with MX-2 600Fe scanning electron microscope(SEM), energy dispersive spectrometer(EDS) and a type of XD-2 X-ray diffractometer(XRD) with Cu K<sub>α</sub> radiation operated at 36 kV and 30 mA was used to analyze the coating phase structure. Micro-hardness along the depth of the cross-section was measured using a MHV2000 type micro Vickers. The load was 1.9614 N and loading time was 10 s. An average value of hardness was taken from five different measurements. Abrasive wear experiments were done without lubrication at the room temperature and normal atmosphere conditions using a friction and wear tester (Model MMS-2A). The ring material of the wear couple was GCr15. The outer radius of the circular test ring was 40 mm. The test specimens were machined with size of 8 mm × 5 mm × 10 mm. The wear conditions were a normal load of 200 N, a sliding speed of 200 r/min, and the time of abrasion of 120 min.

## 3 Results and discussion

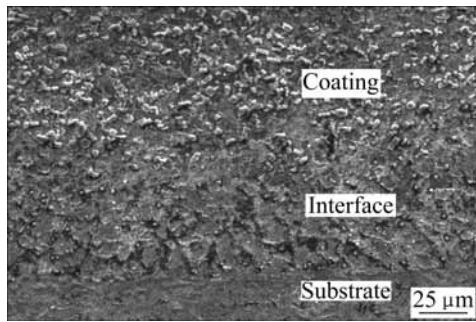
### 3.1 Microstructure

Fig.2 shows the XRD pattern of the locally reinforced Q235 steel composite coating using 70(Ti+B<sub>4</sub>C)-30Fe. The XRD results reveal that the coating mainly consists of TiC, TiB<sub>2</sub> and α-Fe, without TiB and Ti<sub>3</sub>B<sub>4</sub> transient compounds.



**Fig.2** XRD pattern of AAC composite coating

Fig.3 shows the cross-section micrograph of coating. It can be clearly seen that the coating has a good quality, and there are no pores or cracks. The coating has metallurgical bonding with the base material, and the thickness of coating is about 0.8–1 mm. In the interface area, there exists a little reinforcement, conversely there's more in the middle of coatings, where the particles distribute homogeneously. During AAC process, the dilution ratio of the region near substrate is larger than that of the middle region, so there are more particles in the middle area.



**Fig.3** SEM micrograph of coating

Fig.4 reveals a relatively uniform distribution of TiC and TiB<sub>2</sub> in the composite coatings. TiB<sub>2</sub> particles exhibit clubbed shapes, whereas the cubic particulates are TiC. It can be seen from Fig.4, with the increase of (Ti+B<sub>4</sub>C) content, the size of TiB<sub>2</sub> decreases. The volume fraction of TiC-TiB<sub>2</sub> is about 28%–63%, which is calculated by coxpix simple PCI(USA) picture analysis software, and it increases with increasing the mass fraction of (Ti+B<sub>4</sub>C).

Fig.5 shows the scanning electron micrograph of sample 4, together with EDS(see Table 2). It can be seen that the hexagonal and clubbed particles are TiB<sub>2</sub> with the length of 5–10 μm, whereas the cubic and petaloid particles are TiC with the length of 1–3 μm, moreover, most TiB<sub>2</sub> particles have a clubbed structure, and the substrate is α-Fe. The calefactive and refrigerant speeds are very high, and there is some unreacted Ti that

dissolves into α-Fe. The argon arc has large dilution ratio. Together with effect of arc whisking, arc driving and gravity make Fe of base metal come into fused area, which reduces the hardness of coating.

### 3.2 Formation of TiC and TiB<sub>2</sub> particles

A kinetic investigation performed allows us to conclude that solid-state diffusion is the mechanism governing the synthesis process[5,8,19–20]. ZHAO and CHENG[20] suggested two reaction paths:

Path I:



Path II:



At the beginning, B<sub>4</sub>C was surrounded by Ti powders. When the arc reacted with the layer, the layer absorbed much energy and melted quickly. Because Fe has good fusibility and low melting temperature (1 538 °C), it would melt firstly, which made [Ti+B<sub>4</sub>C] immerse into Fe fusant. At the interface between Ti and B<sub>4</sub>C particles, initial atomic diffusion facilitated Ti-containing compounds to form, following reaction(1). The diffusivity of carbon was significantly greater than

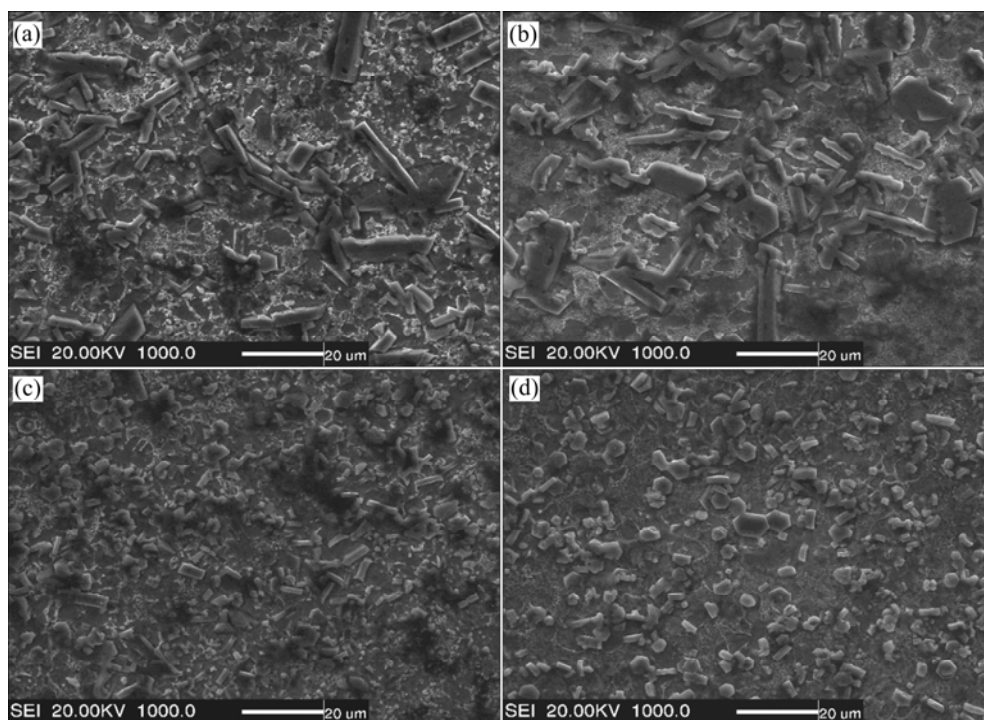


**Fig.4** Typical microstructures of reinforced steel matrix coating fabricated using Fe-Ti-B<sub>4</sub>C systems with different mass fractions of Fe: (a) 70%; (b) 60%; (c) 50%; (d) 30%

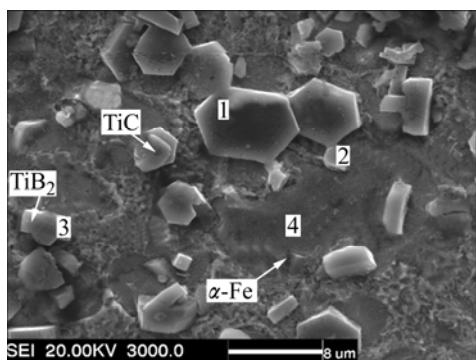


Fig.5 SEM micrograph of coating

Table 2 EDS result (mass fraction, %)

| Zone | Ti    | B     | C     | Fe    |
|------|-------|-------|-------|-------|
| 1    | 28.94 | 71.06 |       |       |
| 2    | 53.11 | 46.89 |       |       |
| 3    | 28.94 | 71.06 |       |       |
| 4    | 1.40  |       | 21.83 | 76.68 |

that of boron[21]. Thus, carbon readily combined with titanium to yield TiC at first. But a concentration gradient of boron existed along the diffusion path between Ti and B<sub>4</sub>C particles, resulting in the formation of TiB. Ti<sub>3</sub>B<sub>4</sub> and TiB<sub>2</sub> phases depended on the mass ratio of Ti to B. At higher temperatures, reaction path I was most likely to become dominant without the transit phase Ti<sub>3</sub>B<sub>4</sub> due to rapid diffusion, leading to a large amount of intermediate phase TiB. Moreover, Ti<sub>3</sub>B<sub>4</sub> was the unstable phase in thermodynamics, which could exist at lower temperature, whereas AAC exhibited high reaction temperature, so we could believe it followed path I in this work. According to XRD, the transit phase TiB converted into TiB<sub>2</sub> absolutely. Fig.6 shows the schematic drawing of the reaction[19].

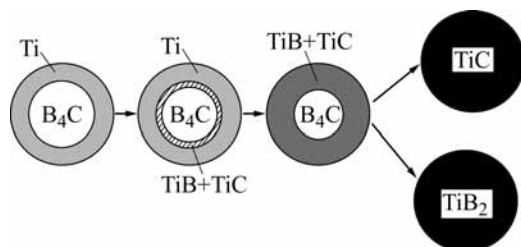


Fig.6 Schematic drawing of reaction

At the beginning of AAC, there was more TiC, and the growth rate of TiB<sub>2</sub> was limited, so TiB<sub>2</sub> grew between the gap of TiC. The TiB<sub>2</sub> that had nucleated early had more time to grow to its crystal structure, which determined the growth pattern as hexagonal prism morphology. With increasing the temperature and holding time, there was more TiB<sub>2</sub>. Most TiB<sub>2</sub> particulates had a clubbed structure because TiB<sub>2</sub>

particulates had enough space to grow amply between TiC particulates. From the XRD pattern, it can be seen that the diffraction peak of TiB<sub>2</sub> is higher than that of TiC. This is consistent with theoretical arithmetic of the following chemical reaction:



### 3.3 Hardness and wear resistance

Fig.7 shows the curves of micro-hardness profiles of AAC samples along the depth of cross-section. It can be seen that with the increase of (Ti+B<sub>4</sub>C) content, the micro-hardness also increases, which is attributed to the increase of hard TiC-TiB<sub>2</sub> ceramic particulates. Sample 4 has the highest hardness, which can reach HV<sub>0.2</sub> 900 four times higher than that of substrate. The surface of coating contacted arc directly, the elements volatilized and overburned seriously, which resulted in the micro-hardness rising from exterior surface to interior, up to the culmination, then decreasing mildly. Between the place of coating and substrate, micro-hardness declines quickly, and reaches the rock bottom at substrate.

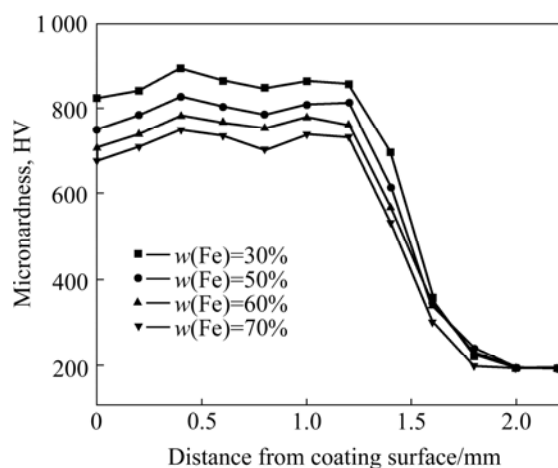


Fig.7 Microhardness curves of AAC

Fig.8 shows the wear loss of composite coatings and Q235 steel. It is clear that wear loss of coatings is smaller than that of Q235 steel, and the wear loss of sample 4 is the smallest, which has the same reason with micro-hardness. It can be seen that: 1) There are many TiC and TiB<sub>2</sub> particulates, which are dispersively distributed in the coating, resulting in dispersion strengthening; 2) AAC has rapid cooling rate, arousing cryptomere strengthening; 3) In-situ TiC and TiB<sub>2</sub> particulates metallurgically bond to the base material; 4) There are many clubbed TiB<sub>2</sub> particulates, which is very useful for improving the mechanical properties of TiC/TiB<sub>2</sub> ceramics[22]. This is because the 1:2 molar ratio of TiC to TiB<sub>2</sub> can weaken the high thermal expansion effect of excessive TiC content and reduce the thermal stresses; however, compared with the formation

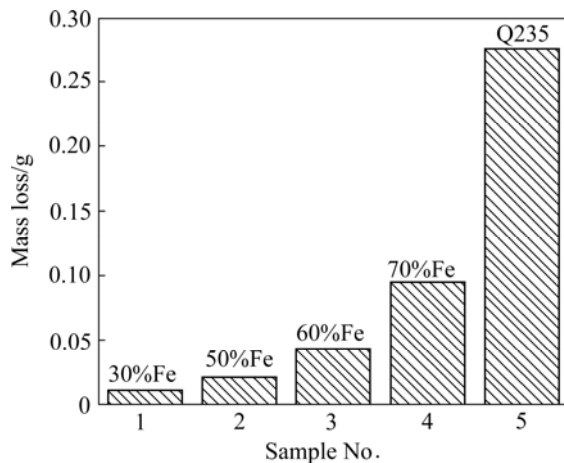


Fig.8 Wear loss of AAC coating and Q235 steel

of pure  $\text{TiB}_2$ , this can decrease the high reaction heat, which can reduce the porosity caused by the gas volatilization[5].

## 4 Conclusions

1) Fe based metallic ceramic coating reinforced by in-situ synthesized  $\text{TiC}$  and  $\text{TiB}_2$  particles was prepared on the surface of Q235 steel by argon arc cladding(AAC) using different mass fractions of Fe and  $\text{Ti+B}_4\text{C}$  powders as the binding materials. The thickness of coating is about 0.8–1 mm. The volume fraction of  $\text{TiC-TiB}_2$  is about 28%–63% and increases with increasing the mass fraction of  $\text{Ti+B}_4\text{C}$ . With the increase of  $\text{Ti+B}_4\text{C}$ , the volume fraction of  $\text{TiC-TiB}_2$  increases as well.

2) Solid-state diffusion is the mechanism governing the synthesis process.  $\text{TiC}$  is the first phase formed, and exhibits cubic and petaloid shapes. While  $\text{TiB}_2$  formation occurs afterward, which presents hexagonal and clubbed forms. And there are not  $\text{TiB}$  and  $\text{Ti}_3\text{B}_4$  transient composites.

3) Sample 4 has the highest micro-hardness and best wear resistance due to more  $\text{TiC-TiB}_2$  ceramic particulates, and the highest hardness is up to  $\text{HV}_{0.2}900$ , four times higher than that of the substrate.

## References

- [1] WANG Xiang, GAI Peng-tao. Effect of carbon content on microstructure and property of  $\text{TiC/Ti-6Al-4V}$  composites [J]. Trans Nonferrous Met Soc China, 2007, 17: s546–s550.
- [2] WU Wang-liang, SUN Jian-feng, DONG Sheng-min, LIU Rong-xiang. Influence of processing parameters on microstructure and wear resistance of  $\text{Ti+TiC}$  laser clad layer on titanium alloy [J]. Trans Nonferrous Met Soc China, 2006, 16: s2096–s2099.
- [3] ZHANG Er-lin, JIN Yun-xue, ZENG Song-yan, ZHU Zhao-jun. Microstructure of in-situ  $\text{TiC}$  particle reinforced titanium alloy matrix composites [J]. Trans Nonferrous Met Soc China, 2000, 6(10): 764–768.
- [4] WANG H Y, HUANG L, JIANG Q C. In situ synthesis of  $\text{TiB}_2\text{-TiC}$  particulates locally reinforced medium carbon steel-matrix composites via the SHS reaction of  $\text{Ni-Ti-B}_4\text{C}$  system during casting [J]. Mater Sci Eng A, 2005, 407: 98–104.
- [5] YANG Ya-feng, WANG Hui-yuan. Fabrication of steel matrix composites locally reinforced with different ratios of  $\text{TiC-TiB}_2$  particulates using SHS reactions of  $\text{Ni-Ti-B}_4\text{C}$  and  $\text{Ni-Ti-B}_4\text{C-C}$  systems during casting [J]. Mater Sci Eng A, 2007, 445/446: 398–404.
- [6] LOCCI A M, ORR'U R, CAO G. Effect of ball milling on simultaneous spark plasma synthesis and densification of  $\text{TiC-TiB}_2$  composites [J]. Mater Sci Eng A, 2006, 434: 23–29.
- [7] ZHAO Kun-yu, ZHU Xin-kun, CHENG Bao-chang, LIN Qiu-shi, ZHANG Xiu-qing, CHEN Tie-li, SHU Yun-shen, YONG Qi-long. Synthesis of  $\text{TiB}_2\text{+TiC}$  by mechanical alloying [J]. Trans Nonferrous Met Soc China, 2001, 11(1): 135–137.
- [8] LOCCI A M, ORR'U R, CAO G, MUNIR Z A. Simultaneous spark plasma synthesis and densification of  $\text{TiC-TiB}_2$  composites [J]. J Am Ceram Soc, 2006, 89: 848–855.
- [9] LEE J W, MUNIR Z A, OHYANAGI M. Dense nanocrystalline  $\text{TiB}_2\text{-TiC}$  composites formed by field activation from high-energy ball milled reactants [J]. Mater Sci Eng A, 2002, 325: 221–227.
- [10] ZHANG Xing-hong, ZHU Chun-cheng, QU Wei-a. Self-propagating high temperature combustion synthesis of  $\text{TiC/TiB}_2$  ceramic-matrix composites [J]. Composites Science and Technology, 2002, 62: 2037–2041.
- [11] HUANG L, WANG H Y, QIU F. Synthesis of dense ceramic particulate reinforced composites from  $\text{Ni-Ti-C}$ ,  $\text{Ni-Ti-B}$ ,  $\text{Ni-Ti-B}_4\text{C}$  and  $\text{Ni-Ti-C-B}$  systems via the SHS reaction, arc melting and suction casting [J]. Mater Sci Eng A, 2006, 422: 309–315.
- [12] KORKUT M H, YILMAZ O, BUYTOZ S. Effect of aging on the microstructure and toughness of the interface zone of a gas tungsten arc(GTA) synthesized  $\text{Fe-Cr-Si-Mo-C}$  coated low carbon steel [J]. Surf Coat Technol, 2002, 157: 5–13.
- [13] EROĞLU M, ÖZDEMİR N. Tungsten-inert gas surface alloying of a low carbon steel [J]. Surf Coat Technol, 2002, 154: 209–217.
- [14] BUYTOZ S, ULUTAN M. In situ synthesis of  $\text{SiC}$  reinforced MMC surface on AISI 304 stainless steel by TIG surface alloying [J]. Surf Coat Technol, 2006, 200: 3698–3734.
- [15] MRIDHA S, ONG H S, POH L S. Intermetallic coatings produced by TIG surface melting [J]. Mater Process Technol, 2001, 113: 516–520.
- [16] WANG X H, SONG S L, ZOU Z D. Fabricating  $\text{TiC}$  particles reinforced Fe-based composite coatings produced by GTAW multi-layers melting process [J]. Mater Sci Eng A, 2006, 441: 60–67.
- [17] WANG X H, SONG S L, QU S Y. Characterization of in situ synthesized  $\text{TiC}$  particle reinforced Fe-based composite coatings produced by multi-pass overlapping GTAW melting process [J]. Surface & Coatings Technology, 2007, 201: 5899–5905.
- [18] BUYTOZ S, ULUTAN M, MUSTAFA Y M. Dry sliding wear behavior of TIG welding clad WC composite coatings [J]. Applied Surface Science, 2005, 252: 1313–1323.
- [19] KLINGER L, GOTMAN I, HORVITZ D. In situ processing of  $\text{TiB}_2\text{/TiC}$  ceramic composites by thermal explosion under pressure: Experimental study and modeling [J]. Mater Sci Eng A, 2001, 302: 92–99.
- [20] ZHAO Hong, CHENG Yi-Bing. Formation of  $\text{TiB}_2\text{-TiC}$  composites by reactive sintering [J]. Ceramics International, 1999, 25: 353–358.
- [21] LASKAR A L, BOCQUET J L, BREBEC G. Diffusion in materials [M]. Netherlands: Kluwer, Dordrecht, 1990.
- [22] ZHANG X H, ZHU C C, QU W. Self-propagating high temperature combustion synthesis of  $\text{TiC/TiB}_2$  ceramic-matrix composites [J]. Comp Sci Tech, 2002, 62: 2037–2041.

(Edited by LI Xiang-qun)